DOI: 10.1002/smll.201201343

Synergetic Material and Structure Optimization Yields Robust Spider Web Anchorages**

Nicola M. Pugno[#], *Steven W. Cranford*[#], *Markus J. Buehler*[*]

[#]Shared first co-authors

Prof. N. M. Pugno
Laboratory of Bio-Inspired Nanomechanics, Department of Structural, Geotechnical and Building Engineering, Politecnico di Torino, Corso Duca degli Abruzzi 24, 10129, Torino, Italy; National Institute of Nuclear Physics, National Laboratories of Frascati, Via E. Fermi 40, 00044, Frascati, Italy; National Institute of Metrological Research, Strada delle Cacce 91, I-10135, Torino, Italy

Mr. S. W. Cranford
Prof. M.J. Buehler
Laboratory for Atomistic and Molecular Mechanics, Department of Civil and Environmental Engineering, Center for Materials Science and Engineering, Massachusetts Institute of Technology, 77 Massachusetts Avenue, Room 1-235A&B, Cambridge, Massachusetts 02139, USA

[*] Corresponding author, mbuehler@MIT.EDU

[**] NMP is supported by the European Research Council under the European Union's Seventh Framework Programme (FP7/2007-2013) / ERC Grant agreement n° 279985 (Ideas Starting Grant BIHSNAM, 2012-2016). NMP and MJB acknowledge the support from the MIT-Italy program MITOR. MJB and SWC acknowledge support from a NSF-MRSEC grant with additional support from ONR, AFOSR and ARO. The authors thank J. Vanzo for discussion.

Supporting Information is available on the WWW under http://www.small-journal.com or from the author.

Keywords: Adhesion, microscale, silk; optimization; hierarchical, biological material; biomimetics

Abstract: *Millions of years of evolution have adapted spider webs to achieve a range of properties, including the well-known capture of prey, with efficient use of material. One feature that remains poorly understood is the attachment disc, a network of silk fibers that mechanically anchors a web to its environment. Experimental observations suggest that the attachment disc adheres to the substrate through multiple symmetrically branched structures composed of sub-micrometer scale silk fibers. Here we use a theoretical model to explore the adaptation of the strength of attachment of such an anchorage, and apply complementary mesoscale simulations to demonstrate a novel mechanism of synergetic material and structural optimization, such that the maximum anchorage strength can be*

achieved regardless of the initial anchor placement or material type. We find that the optimal delamination (peeling) angle is facilitated by the symmetry and inherent extensibility of silk, and is attained automatically during the process of delamination. This concept of self-optimizing peeling angle suggests that attachment discs do not require precise placement by the spider, irrespective of adhesion strength. Additional hierarchical branching of the anchorage increases efficiency, where both the delamination force and toughness modulus increase with a decrease in cross-sectional area.

1. Introduction

Spider webs are fascinating examples of natural structural engineering essential for an animal's survival.[1] It is well known that silk displays exemplary mechanical properties,[2] but less clear is by which mechanism the web is attached to its environment. The evolutionary demands placed on spiders[3] are reflected in the design of their webs, both structurally and from a materials perspective.[4] Natural web architectures provide an inspiration to structural engineers,[5] and matching the remarkable properties of silk fibers presents a challenge to materials scientists.[6] Recent work suggests that the separate consideration of structure and material is insufficient.[7] While it has been shown that webs themselves are robust and flaw tolerant,[4, 8] how precise must a spider construct the structures that attach a web to its environment? Uncertainty and variation in environmental conditions suggest a need for robust and adaptable anchorages, yet webs illustrate reproducible and deliberate geometric construction. Here we report a study which examines the mechanism of itegrated optimization of material and structure via a detailed analysis of the attachment disc,[9] the structure used to anchor webs to their physical surroundings (cementing dragline silks to a solid supports such as wood, concrete, or other surfaces during web construction). Dragline silk, which is often referred to as a "safety line" for the spider[10] has been observed to fuse with attachment disc silk, providing dragline silk with a secure anchor point to assist prey capture and predator evasion.[9]

The splayed attachment disc displays remarkable adhesive properties and holds great potential to guide the design of bio-inspired and biomimetic anchorages and adhesives.[11] The morphological convergence of hierarchical branched adhesive pads in lizards, spiders and several insect orders, for example, indicates an advantage of this design for substrate adhesion.[12] Due to the physiological role, the problem of branched adhesion has been investigated previously from the perspective of attachment and detachment cycles and related biomechanical functions.[11, 13] Moreover, early functional explanations of such adhesive organs focused on the performance on rough substrates, where flexible branched fibers can make more intimate contact, control detachment and increase adhesion.[12c, 14] In contrast, the attachment disk of a spider web is a *passive* structure, wherein secure attachment (optimal adhesion) is the primary goal, subsidiary to ease of detachment. Unlike the gecko's foot, for example, the attachment must provide a permanent anchorage of a spider's web upon construction. As such, the analysis and computational experiments focus on peeling strength and toughness to investigate the material and structural synergy of the anchorage. Little is known about the intricate, lace-like structure of the attachment disc (**Figure 1a**) or the mechanical properties of the piriform silk that compose it.[3, 15] Yet, the hierarchical arrangement of the anchorage, wherein a single silk thread is splayed into numerous contact fibers, shares some similarity to the gecko's foot.[13]

2. Theoretical Results and Discussion

We consider the structure depicted in **Figure 1b** that shows a model of a simple anchorage to reflect the geometry identified in SEM imaging. A simple anchorage is defined as a colarchic, two-branched, symmetrical, adhesive anchorage. It is an adhesive anchorage because it allows a force, F, to be transmitted to a solid substrate through adhesive forces at the material interface (e.g., no penetration of material entanglement), symmetrical because the angles, α, on both side are equal, and it is colarchic because it has no hierarchy. The model represents the most basic geometry of anchorages that engage

adhesive forces at the structure-substrate interface. It is used here as the starting point for a systematic analysis based on the theory of multiple peeling.[16]

2.1 Optimal Angle

In an earlier work[16] we proposed an elastic theory model of the simple anchorage with adhesive forces at the branch-substrate interface, and found that the critical delamination force is:

$$F_{\mathrm{d}} = 2YA_{\mathrm{c}}\sin\alpha\varepsilon_{\mathrm{d}} \quad (1)$$

where Y is the elastic modulus, A_{c} is the branch cross-sectional area and $\varepsilon_{\mathrm{d}}$is the critical level of strain at which a branch will delaminate. Balancing the critical delamination force, strain, and adhesion energy, and contact angle, yields:

$$\varepsilon_{\mathrm{d}} = \left[\cos(\alpha) - 1 + \sqrt{\left(1-\cos(\alpha)\right)^2 + \lambda}\right], \quad (2)$$

where ε_{d} is the critical level of strain to initiate delamination, and α the contact angle.[16] We introduce a nondimensional parameter, λ, representing the competition between adhesion energy per unit length, γ, and elasticity ($\lambda = 4\gamma/(YA_{\mathrm{c}})$; where Y is the elastic modulus and A_{c} is the cross-sectional area of a branch). Hence, the contact angle α is a parameter that can change the critical delamination force through strain (ε_{d} decreases as $\alpha\rightarrow 90°$). This is similar to the geometrically induced attachment/detachment trigger of the gecko's seta, [13, 17] facilitated by the unidirectionality and cooperativity of the seta. Silk anchorages, however, are multi-branched in varied directions, increasing the contact angle on one adhered branch subsequently decreases the angle of the opposite. Therefore,

for stable anchorage of spider webs, directionally opposed pairs minimize the loss of adhesion due to geometric changes in the angle. More importantly, we find that an optimal contact angle, α_{max}, maximizes the delamination force and depends on λ.

There exists an optimal angle, α_{max}, that maximizes the delamination force and is dependent on λ. Substituting Equation (2) into (1) for ε_d, finding where the derivative of the structural delamination force with respect to α is equal to zero corresponding to a force maximum:

$$\frac{dF_d}{d\alpha} = 2YA_c\left[\cos\alpha\left(\cos\alpha - 1 + \sqrt{(1-\cos\alpha)^2+\lambda}\right) + \sin\alpha\left(-\sin\alpha + \frac{(1-\cos\alpha)\sin\alpha}{\sqrt{(1-\cos\alpha)^2+\lambda}}\right)\right] = 0 \qquad (3)$$

from which we derive:

$$\cos(\alpha_{max}) = \frac{1}{\cos(\alpha_{max}) + \sqrt{\left(1-\cos(\alpha_{max})\right)^2+\lambda}} = \frac{1}{1+\varepsilon_d}. \qquad (4)$$

We note that $\alpha_{max} \to 90°$ as the material becomes increasingly compliant ($\varepsilon_d \to \infty$), while $\alpha_{max} \to 0°$ with an increase in stiffness ($\varepsilon_d \to 0$). This result also implies that the force required for delamination is geometrically restricted by the contact angle, α_{max}. A fixed peeling angle, α, enables the variation of delamination force from a negligible to a very significant value. A single adhered branch with a free end can be delaminated with lower force with induced variation in geometry. Indeed, it is has been shown that the unique macroscopic orientation and preloading of the gecko seta can successfully increase attachment force, while suitably orientated setae can reduce the forces necessary to peel the toe by simply detaching above a critical angle with the substrate[13, 17] – a geometrically induced attachment/detachment trigger. However, this mechanism is facilitated by the unidirectionality and

cooperativity of the gecko's seta[13, 17] – a feature not present in the two-branched anchorage. Variation in attachment angle can not be easily achieved without initiating delamination – increasing the contact angle on one adhered brance subsequently decreases the angle of the opposite. Thus for *stable* anchorage, directionally opposed pairs minimize loss of adhesion due to geometric changes in angle.

2.3 Synergetic Optimization of Structure and Material

The design of the anchorage can be optimized by stipulating that material failure and delamination occur at the same load, similar to the principle of optimal design of laminate composites wherein all layers in the composite are designed to fail simultaneously – no material strength is left unused. This implies comparable probabilistic failures of the attachment discs and silk fibers in agreement with observations in preliminary experiments conducted on spider webs. The strictly economic design principles that have been noted in the architecture of spider webs[2a, 3, 18] are necessary for a creature that internally produces all of its own building material. That the spider web uses a remarkably tiny volume of material to cover a relatively broad area is an evident example of this type of economy, but volume of material may not be the only measure of cost; we note that recent research found that the great strength of major ampullate silk fibers, such as dragline silk, is due to nanoscale β-crystals.[19] We suppose that the production of these super-strong crystals might have an extra cost to the spider-one which would be purely wasteful in a condition where an incongruency between adhesive and strength failure leaves the strength capacity unused.

Setting the delamination strain to equal the material's ultimate strain (ε_{p}), we pose the condition of simultaneous failure where $F_{\mathrm{p}}^{\mathrm{opt}} = F_{\mathrm{d}}$ and as a result $\varepsilon_{\mathrm{p}}^{\mathrm{opt}} = \varepsilon_{\mathrm{d}}$. Equations (2) and (4) can therefore be rewritten to relate the optimal material strain ($\varepsilon_{\mathrm{p}}^{\mathrm{opt}}$) to the optimal angle ($\alpha_{\max}$):

$$\varepsilon_{\mathrm{p}}^{\mathrm{opt}} = \frac{1}{\cos(\alpha_{\max})} - 1 \quad (5)$$

Equation (5) shows that material behaviour elicits a particular structural optimization, and a direct relation between λ and ε_{p} can be found from Equation (2):

$$\lambda^{\mathrm{opt}} = \left(\varepsilon_{\mathrm{p}}^{\mathrm{opt}}\right)^2 + 2\varepsilon_{\mathrm{p}}^{\mathrm{opt}}\left(1 - \frac{1}{1+\varepsilon_{\mathrm{p}}^{\mathrm{opt}}}\right). \quad (6)$$

Equations (5) and (6) describe simultaneous structural (α^{opt}, λ^{opt}) and material ($\varepsilon^{\mathrm{opt}}$) optimizations.

Among the types of silk found in spider webs, it has been noted that dragline and flagelliform silks absorb more energy prior to failure than almost any commonly used material.[3] If we define energetic capacity as the elastic energy until failure as T (toughness modulus), we can relate the optimal energetic capacity, strength, and strain (see **SI Section S1** for derivation). We find that $T^{\mathrm{opt}} \sim \varepsilon_{\mathrm{p}}^{\mathrm{opt}}$, whereas $F^{\mathrm{opt}} \sim 1/\varepsilon_{\mathrm{p}}^{\mathrm{opt}}$. This relation indicates a second benefit to compliance (*i.e.*, increased detachment strain), whereby the energy capacitance increases to maximize the adhesion (*e.g.*, $T^{\mathrm{opt}} \rightarrow 4\gamma L$ as $\varepsilon_{\mathrm{p}}^{\mathrm{opt}} \rightarrow \infty$) under simultaneous material failure and delamination. Note that this does not hold for simple detachment - as previously stated, the relative stiffness of the gecko's toe allows for easy detachment by inducing the critical angle required for delamination – it is presumed the gecko does not want a toe to fracture simultaneously.

The definition of toughness illustrates a trade-off where high values of ε_{p} lead to a relatively high

energetic capacity and a relatively low force capacity, while for low values of ε_p the opposite is true. Polymeric adhesives (such as tapes) are preferably soft such that able to deform sufficiently for intimate contact over a relatively large surface area and maximize adhesion.[20] Indeed, when two materials are brought into contact, their surface roughness is crucial to determine the quality of contact and hence the intensity of adhesion (similar to why household tape sticks better by pushing it into a contact with a surface). The same benefit can be associated with the silk attachment disc, flexible and extensible threads can easily adapt to the topography of rough substrates and achieve a more intimate contact, and thus compliant silk is beneficial.

2.4 Hierarchical Branching: Thinner is Stronger

Inspired by the vast number of tiny anchorages of which the attachment disc is composed (see **Figure 1a**), we pose the question: is there an advantage in a greater number of attachments? A similar scaling effect was exploited earlier by introducing the principle of contact splitting,[12b] whereby dividing a structure into finer subcontacts increases adhesion.[16] If adhesive forces scale linearly with the dimensions of the contact, as they do here, the adhesive strength scales with the peeling edge length and not with the area.[12a, 12b]

Extending this concept, as an alternative to the simple structure with two branches, we consider an analogous structure with 2N symmetrical branches with equivalent cross-section (**Figure 1c**). The structural force and energy capacity can be rewritten in terms of the constant volume, $V=2Na_cL$. For a thread of constant volume and length both energy capacity, T, and strength, F, increase with a decrease in cross-sectional area, a_c (see **SI Section S2** for details of the derivation). If we consider a film-like cross-sectional area, where $a_c = hw$, (h = height; w = contact width) we see, along with decreasing w, that the force and toughness modulus increase with a decreasing height of the thread or branch, h. As a

result, given a peeling edge of constant width, a decrease in branch height, without changing the contact interface, results in increased performance, similar to the effect observed in contact splitting. This can be justified through the nondimensional parameter λ, representing the balance of elastic and adhesion, which can be altered through h alone, regardless of w. Hence the performance of the anchorage can be optimized by having a cross-section as thin as possible, whether this means using 2 or N branches.

2.5 Piriform Silk Sequence: Evidence of Extensibility

The mechanical analysis of this simple anchorage model also lends insight into the unknown mechanical behavior of piriform silk. SEM data support the notion that the spigots of the piriform gland are relatively small but numerous, and are located near the major ampullate spigots on the same spinneret.[21] We know that piriform spigots are present in most if not all orb-weaving species,[22] and recent studies have identified its protein sequence for the cob-weaving *L. hesperus* (black widow spider),[9] the orb-weaving *A. trifasciata* (banded garden spider), *N. clavipes* (golden silk spider), as well as for *N. cruentata.*[23]

Direct mechanical characterization of piriform silk and the attachment disk has yet to be reported. However, recent research into the sequence of the piriform silk proteins can be compared to mechanical cues derived from investigations of dragline silks.[19a, 19c] For example, major ampullate proteins that forms dragline silk are composed of polyalanine sequences and glycine-rich domains which form the secondary structure of the protein.[24] The polyalanine sequences form β-sheet nanocrystals, which endow dragline silk with high strength [19a, 19c, 25] while the remaining glycine-rich amorphous sections enhance the material's extensibility.[24c] In contrast, two studies of the sequence of piriform silk from three orb-weaving species (*A. trifasciata*, *N. clavipes*, and *N. cruentata*) revealed

two new repeat motifs, named PXP and QQ, which have not been found in any other spider silk protein sequences.[23] It was proposed that the QQ amino acid motifs, a periodic arrangement of polar and nonpolar residues, could form surfaces well-suited for both hydrophobic and hydrophilic interactions,[23] extending possible successful anchorage sites. Additionally, although the translated sequence predicted substantial amounts of alanine amino acids, no long polyalanine stretches were identified.[26] Instead, short runs of three consecutive alanine residues appeared in a regular pattern within sequence. This suggests that the piriform silk may lack a well-defined β-sheet nanocrystalline structure that controls the high strength of dragline silks, and may rather be dominated by the semi-amorphous behavior, leading to great extensibility and hyperelastic stiffening.[19a]

By making use of both the SEM photograph of the attachment disc of a black widow spider[9] (**Figure 1a**) and our theoretical model we make a first order approximation of the properties of piriform silk (**SI Section S3**). Estimating the number of contacts depicted, a stiffness (≈3 MPa, on the order of the values measured for capture (or viscid) silks[10]) and an energy of adhesion (≈10 N/m), we estimate the piriform silk extensibility to be on the order of ≈3.4 (through Equation (4) and Equation (5)). We note that this material extensibility is relatively high, but is supported by the aforementioned lack of polyalanine sequences in the protein. A similar range of high extensibilities have been measured in capture (or viscid) silks.[27] It is noted that these values represent only a rough initial estimation of the properties of piriform silk.

3. Computational Results and Discussion

While the exact mechanical behavior is piriform silk is unknown, it does not eliminate the possibility to explore the behavior of the attachment disc using a series of computational experiments. While unnecessary to model the exact behavior of piriform silk constituting the attachment disc, we wish to

accurately capture the generic silk-like behavior and assess the mechanisms of detachment. Thus, for the current investigation, as a simplification, we implement general models previously developed for dragline and viscid silks (see **Figure S1** and **Methods**).

3.1 Simulated two-branch peeling

We first model a silk strip as a two-branched anchorage with varying initial angle (α_0 = 15°, 30°, 45°, 60°, and 75°, subject to an increasing vertical force see (**Figure 2a**). Upon loading, we measure the attachment angle and applied force (examples plotted in **Figure 2b-c**). Initially there is deformation without delamination; and the angle increases. This initial change in geometry is facilitated by the inherent yielding and softening of the silk, and there is a large change in angle at a marginal applied force. Once the detachment process reaches a certain angle it maintains that angle by delaminating and deforming upwards in equal measure. Moreover, we observe that the angle evolves towards an asymptotic value which is the same regardless of the initial angle used (see **Figure 2c**). This means that the two-branched adhesive anchorage, laid down with an arbitrary initial angle, modifies itself with pulling towards an "intrinsic" structural angle. This asymptotic angle, α_∞, coincides with the critical angle in delamination, α_{max}, as described by Equation (4). We note that it varies with the value of the adhesion parameter, γ_L, which is an input in our model (**Figure 2b-c**). We subsequently calculate the value of λ (see **SI Section S4** for details), where λ is used to find the theoretical values of the optimal angle, α_{max}, through Equation (4). The measured values of F_{silk} and α_{max} are reported in **Table 1**. We find an excellent agreement between the asymptotic angles seen in our simulations and the theoretical critical delamination angle.

To demonstrate that the optimization occurs irrespective of the nonlinear behavior of silk, we introduce additional general constitutive material laws such that strain at delamination is variable (through

parameterization of stiffness and ultimate strain, but constant strength). We employ a general hyperelastic model with ultimate strains ranging from 0.1 (stiff) to 10 (extensible), with a constant substrate adhesion strength (γ_L=10 μJ/m) and initial contact angle (α_0 = 45°). Again, upon load, there is deformation without delamination inducing an angle increase, regardless of the model (**Figure 2d**). Detachment is initiated at different angles (and, equivalently, forces; not shown), followed by convergence to an asymptotic angle, which varies as a function of extensibility (measured angles range from 51.6° at $\varepsilon_d \approx$ 0.05 to 80.6° at $\varepsilon_d \approx 5.0$). Simply put, for the same required delamination force, more compliant silk reaches a higher delamination strain, and thus a higher peeling angle. We further note that the optimal angle, α_{max}, is not reached for the general hyperelastic model employed (**Figure 2d)**. Indeed, upon delamination, the detached silk subject to load has little intrinsic stiffness, and the subsequent strain results in deviation from the optimal angle – the upward pulling of the thread can only increase the local peeling angle. This effect is amplified for stiff silks, where the difference in stiffness changes dramatically with strain. For the previous nonlinear model, the effect was negated by the initial silk stiffness prior to yield – the detaching segments are intrinsically stiffer than the free thread. In both cases, for optimal performance, extensibility of the attachment silk is an asset. The simulation of different materials verifies the validity of Equation (5) as the relation between optimal delamination strain and angle, and thus applicable considering the real, currently unknown, material behavior of the attached silk anchorage. We further conclude that self-optimization cannot be reached for stiffer silks, as the dynamic peeling process cannot converge to the ideal angle.

Our simulations reveal an interesting property of "self-optimization"- under load the anchorage automatically approaches the optimal configuration, by either increasing or decreasing the attachment angle. Notably, this behavior is facilitated by the intrinsic extensibility of the silk, allowing the freedom to reconfigure angles of attachment with little applied load, followed by increase in stiffness after the

optimal angle is attained under stress. For the purely hyperelastic cases (no yield), attaining the optimal delamination angle was hindered by the stiffness of the silk, yet each material case was "self-optimizing". Although the current model is simplified compared to the complex structure of the attachment disc, the concept of "self-optimization" of adhesive anchorages provides a possible explanation for how 10,000 connections might be able to conform to function in a precise optimal configuration.

3.2 Detachment Under Wind Loading

Common loading scenarios in a web's natural environment are forces caused by wind, and web anchorages should adequately transfer any anticipated wind loads without detachment. For a given wind speed, U, we calculate the effective drag force on a web per anchorage, F_{wind}. We assume symmetric resistance of the force, wherein each supporting radial assumes an equal fraction of the load. From these simplifying assumptions, we relate wind speed (U) to applied anchorage force (F_{wind}), depicted schematically in **Figure 3a**. The structure is then subject to a constant force allowing a conformational change until equilibrium is reached. There are three possible outcomes: (1), adhesion energy is sufficient to resist the applied force, and the structure equilibrates to a finite displacement (**Figure 3b**); (2), adhesion energy is inadequate, and delamination occurs; (3), adhesion energy is sufficient to prevent delamination, but ultimate stress (fracture) is reached in the anchor. The wind speed is systematically increased until failure by delamination occurs. Once delamination occurs, the adhesion energy is incrementally increased and the anchorage subject to further increases in applied force. This process is repeated until fracture of the threads is the failure mode (**Figure 3c**).

The mode of failure is investigated for adhesion energies ranging from γ_L = 10 μJ/m to 150 μJ/m. At small adhesion energies, delamination occurs at relatively small wind speed (delamination for winds in

exceeding 20 m/s for γ = 10 μJ/m, for example). The plot depicted in **Figure 3c** is reflective of the constitutive stress-strain relationship for the model silk (*e.g.*, yielding and subsequent hyperelastic stiffening occurring at wind speeds >10 m/s). The simplified assumptions (such as number of anchoring radial threads, the total length of silk in a web, and the number of adhesive branches per radial thread) limit a more exact prediction of adhesion energy, but provide a realistic range subject to experimental validation and a means to systematically vary the applied load. A more refined prediction of adhesion strength is unsubstantiated, considering the approximated constitutive law and the idealized fiber-substrate interaction. Variation in substrate and environment anchoring conditions (such as material chemistry, surface roughness, temperature, humidity, etc.) prohibit any single specific adhesion energy. Such uncertainties support the self-optimizing design of a two-branched anchorage system.

In spite of such contingencies, the computational results indicate a range of adhesion strengths in a physically reasonable regime. While the constitutive relation employed is representative of major ampullate dragline silk, the attainable ultimate stress and strain is within the same order of magnitude as other, empirically characterized silks.[27a, 28] Increasing adhesion energy can prevent delamination further, limited by ultimate failure (fracture) of the anchor threads, occurring when the adhesion energy is on the order of 150 μJ/m (subject to the limiting strength of the model silk, ≈1,400 MPa). Thus, this value ultimate sets the upper bound for predicted adhesion energy, based simply on the ultimate stress of the dragline threads. A value of adhesion energy on the order of 150 μJ/m is optimal uniformly strong silk anchorages (simultaneous delamination and rupture). In addition, for the current silk anchorage model, the yield occurs at wind speeds exceeding 10 m/s, defining a reasonable regime of operational wind speeds, below which structural integrity of a web anchorage is maintained. Interspecies variation of this yield point[28] may predict the wind conditions a web is subjected to.

4. Conclusion

We have demonstrated an intrinsic optimization mechanism of a spider web attachment disc using an elastic theory model of a multiple branch adhesive anchorage, validated by computational modeling and combined with an analysis of its natural structure. Hypothesizing that the attachment disk of the spider web must be designed with two functionalities: *i.e.* force capacity and energetic capacity, and with minimal material, we demonstrated optimization of the structure using an elastica theory model of a multiple branch adhesive anchorage. While similar to the hierarchical branched adhesive pads in lizards, spiders and several insects, the attachment disk employed by the spider exploits a different set of mechanistic principles. As the spider is both a structural engineer and a materials scientist, the optimization is both structural and material. Structurally, a balance of the delamination force (F_d) and strain (ε_d) results in an intrinsic optimal delamination (or peeling) angle (α_{max}) which maximizes the adhesion strength of the anchorage. A potential tunable variable for other biological adhesive systems (such as the gecko's seta), this maximizing angle is facilitated by the initial two-branched V-shape of the attachment disk, and symmetric yet opposing directionality of the fibers in contact with the substrate. While investigations contact splitting has elucidated the benefits of multiple adhesion threads [12b-d], and the angle of peeling has been delinated as a critical delamination parameter [13, 17], the coupling of hierachical branching, cooperative delamination, and the convergence to optimal angle is a key insight revealed by the spider's attachment disk. Moreover, from a materials perspective, the inherent extensibility of silk acts as a natural guide, allowing the the structural arrangement of the anchorage to reconfigure and "find" the optimal angle under load, regardless of initial geometry, suggesting such attachements do not require precise placement by the spider *in situ*. As a result, little effort is needed to survey potential (successful) anchorage sites. It seems Spiderman's nonchalant targeting of Manhattan skyscraper ledges to adhere his web has biological evidence – the attachment

will naturally optimize upon load. Indeed, rather than redesign, a spider employs an anchorage that, while not universal, can adequately perform under a range of conditions.

Our model further suggests that piriform silk is an extremely extensible and compliant fiber, perhaps similar to an elastic polymer such as natural rubber. This agrees well with recent sequencing efforts, which show that the piriform silk protein lacks repeating polyalanine segments than result in the β-sheet nanocrystalline structure (and strength and stiffness) of dragline silks. We further estimate a range of adhesion strengths of 10 μJ/m to 150 μJ/m (assuming a fracture stress of ≈1 GPa). Achieving similar properties would be highly desirable for synthetic biomimetic fibrillar adhesives, with potential applications in including micro- and nanomanipulation in production processes, microelectronics, biomedicine and robotics.

5. Methods

Full details of methods are included in the SI part of the paper; here we include a brief summary of the key methods used. To capture the general structural behaviour of the anchor, the constitutive behavior of silk is parameterized based on full atomistic simulations of dragline spider silk[19a, 19c] to formulate generic nonlinear models with realistic ultimate stress (depicted in **Figure S1** see **SI Section S5),** comparable to experimental findings.[10] We implement this silk model using LAMMPS[29] (http://lammps.sandia.gov/), modified to reflect the stress-strain relations of silk. We use Steered Molecular Dynamics[30] (SMD) with a constant pulling velocity as the protocol for simulating the force-induced deformation of attachment structure. The SMD approach applies a moving spring force (pulled at a constant rate of 0.05 mm/s and with a spring stiffness of 0.1 N/m), such that the structure can behave in a manner not captured by either force or displacement loading alone, allowing induced conformational changes in the system. We introduce a single silk thread with a total length of 45 mm,

of which 40 mm (two 20 mm branches) is attached to a rigid substrate through Lennard-Jones interactions (see **SI Section S6**). To approximate equivalent wind loading, the force transferred to each two branch anchorage was calculated as the effect of drag on the silk threads of a presumed web structure (see **SI Section S7**). The total drag force is calculated assuming the total area of radial and spiral threads in an orb web (inset; here eight radials support the spiral structure) and a constant wind speed, U. The total force is then divided equally among the anchoring radial threads (n = 8), which are presumed to branch into adhered anchorages (conservation of area).

---

[1] Hansell, M. H., *Animinal architecture, 1st edn.* Oxford University Press: New York, NY, **2005**.
[2] a) Gosline, J. M.; Demont, M. E.; Denny, M. W., *Endeavour* **1986,** *10* (1), 37-43; b) Ko, K. K.; Kawabata, S.; Inoue, M.; Niwa, M.; Fossey, S.; Song, J. W., *Advanced Fibers, Plastics, Laminates and Composites* **2002,** *702*, 17-23.
[3] Lewis, R. V., *Chem Rev* **2006,** *106* (9), 3762-3774. DOI Doi 10.1021/Cr010194g.
[4] Cranford, S. W.; Tarakanova, A.; Pugno, N. M.; Buehler, M. J., *Nature* **2012,** *482* (7383), 72-U91. DOI Doi 10.1038/Nature10739.
[5] Carpinteri, A.; Pugno, N. M., *J Phys-Condens Mat* **2008,** *20* (47). DOI Artn 474213 Doi 10.1088/0953-8984/20/47/474213.
[6] a) Bosia, F.; Buehler, M. J.; Pugno, N. M., *Phys Rev E* **2010,** *82* (5). DOI Artn 059902 Doi 10.1103/Physreve.82.059902; b) Pugno, N. M., *J Phys-Condens Mat* **2007,** *19* (39). DOI Artn 395001
Doi 10.1088/0953-8984/19/39/395001.
[7] a) Agnarsson, I.; Blackledge, T. A., *J Zool* **2009,** *278* (2), 134-140. DOI DOI 10.1111/j.1469-7998.2009.00558.x; b) Sensenig, A.; Agnarsson, I.; Blackledge, T. A., *J Evolution Biol* **2010,** *23* (9), 1839-1856. DOI DOI 10.1111/j.1420-9101.2010.02048.x; c) Opell, B. D.; Bond, J. E., *Evolutionary Ecology Research* **2001,** *3* (5), 567-581.
[8] Aoyanagi, Y.; Okumura, K., *Physical Review Letters* **2010,** *104* (3).
[9] Blasingame, E.; Tuton-Blasingame, T.; Larkin, L.; Falick, A. M.; Zhao, L.; Fong, J.; Vaidyanathan, V.; Visperas, A.; Geurts, P.; Hu, X. Y.; La Mattina, C.; Vierra, C., *J Biol Chem* **2009,** *284* (42), 29097-29108. DOI DOI 10.1074/jbc.M109.021378.
[10] Gosline, J. M.; Guerette, P. A.; Ortlepp, C. S.; Savage, K. N., *Journal of Experimental Biology* **1999,** *202* (23), 3295-3303.
[11] Pugno, N. M., *Nano Today* **2008,** *3* (5-6), 35-41.
[12] a) Varenberg, M.; Pugno, N. M.; Gorb, S. N., *Soft Matter* **2010,** *6* (14), 3269-3272. DOI Doi 10.1039/C003207g; b) Arzt, E.; Gorb, S.; Spolenak, R., *P Natl Acad Sci USA* **2003,** *100* (19), 10603-10606. DOI DOI 10.1073/pnas.1534701100; c) Gao, H. J.; Yao, H. M., *P Natl Acad Sci USA* **2004,** *101* (21), 7851-7856. DOI DOI 10.1073/pnas.0400757101; d) Filippov, A.; Popov, V. L.; Gorb, S. N., *J Theor Biol* **2011,** *276* (1), 126-131. DOI DOI 10.1016/j.jtbi.2011.01.049.
[13] Autumn, K.; Liang, Y. A.; Hsieh, S. T.; Zesch, W.; Chan, W. P.; Kenny, T. W.; Fearing, R.; Full, R. J., *Nature* **2000,** *405* (6787), 681-685.

[14] Federle, W., *Journal of Experimental Biology* **2006,** *209* (14), 2611-2621. DOI Doi 10.1242/Jeb.02323.
[15] Vollrath, F.; Knight, D. P., *Nature* **2001,** *410* (6828), 541-548.
[16] Pugno, N., *International Journal of Fracture* **2011,** *DOI: 10.1007/s10704-011-9638-2*.
[17] Tian, Y.; Pesika, N.; Zeng, H. B.; Rosenberg, K.; Zhao, B. X.; McGuiggan, P.; Autumn, K.; Israelachvili, J., *P Natl Acad Sci USA* **2006,** *103* (51), 19320-19325. DOI DOI 10.1073/pnas.0608841103.
[18] Opell, B. D., *Funct Ecol* **1998,** *12* (4), 613-624.
[19] a) Keten, S.; Buehler, M. J., *Journal of The Royal Society Interface* **2010**; b) Nova, A.; Keten, S.; Pugno, N. M.; Redaelli, A.; Buehler, M. J., *Nano Lett* **2010,** *10* (7), 2626-2634. DOI Doi 10.1021/Nl101341w; c) Keten, S.; Xu, Z. P.; Ihle, B.; Buehler, M. J., *Nature Materials* **2010,** *9* (4), 359-367.
[20] Gay, C.; Leibler, L., *Physical Review Letters* **1999,** *82* (5), 936-939.
[21] Moon, M.-J.; An, J.-S., *Entomological Research* **2006,** *36* (3), 133-138.
[22] Coddington, J. A., *J Arachnol* **1989,** *17* (1), 71-95.
[23] Perry, D. J.; Bittencourt, D.; Siltberg-Liberles, J.; Rech, E. L.; Lewis, R. V., *Biomacromolecules* **2010,** *11* (11), 3000-3006. DOI Doi 10.1021/Bm1007585.
[24] a) Simmons, A.; Ray, E.; Jelinski, L. W., *Macromolecules* **1994,** *27* (18), 5235-5237; b) Kummerlen, J.; van Beek, J. D.; Vollrath, F.; Meier, B. H., *Macromolecules* **1996,** *29* (8), 2920-2928; c) Lefevre, T.; Rousseau, M. E.; Pezolet, M., *Biophysical Journal* **2007,** *92* (8), 2885-2895; d) van Beek, J. D.; Hess, S.; Vollrath, F.; Meier, B. H., *P Natl Acad Sci USA* **2002,** *99* (16), 10266-10271.
[25] a) Fossey, S. A.; Nemethy, G.; Gibson, K. D.; Scheraga, H. A., *Biopolymers* **1991,** *31* (13), 1529-1541; b) Xiao, S. B.; Stacklies, W.; Cetinkaya, M.; Markert, B.; Grater, F., *Biophysical Journal* **2009,** *96* (10), 3997-4005. DOI DOI 10.1016/j.bpj.2009.02.052.
[26] Ayoub, N. A.; Garb, J. E.; Tinghitella, R. M.; Collin, M. A.; Hayashi, C. Y., *Plos One* **2007,** *2* (6). DOI ARTN e514
DOI 10.1371/journal.pone.0000514.
[27] a) Swanson, B. O.; Blackledge, T. A.; Hayash, C. Y., *J Exp Zool Part A* **2007,** *307A* (11), 654-666. DOI Doi 10.1002/Jez.420; b) Lepore, E.; Marchioro, A.; Isaia, M.; Buehler, M. J.; Pugno, N., *PLos One (in submission)* **2011**.
[28] Agnarsson, I.; Kuntner, M.; Blackledge, T. A., *Plos One* **2010,** *5* (9).
[29] Plimpton, S. J., *Journal of Computational Physics* **1995,** *117*, 1-19.
[30] Sotomayor, M.; Schulten, K., *Science* **2007,** *316* (5828), 1144-1148. DOI DOI 10.1126/science.1137591.

Tables and Table Captions

Table 1: Comparison of asymptotic simulation angles and delamination forces with theoretically predicted optimum angles and force.

Substrate adhesion strength (J/m)	**Asymptotic detachment angle**	**Applied delamination force (μN)**	**Simulated delamination strain**	**Energy balance parameter**	**Optimal detachment angle**	**Optimal detachment force (μN)**
γ_L	α_∞	$F_{silk} = F_d$	ε_d	λ	α_{max} **[Eq. (4)]**	F_1^{opt}
0.2×10^{-5}	34.74°	19.5	0.2150	0.101	33.14°	15.9
1×10^{-5}	46.82°	62.0	0.4910	0.462	46.01°	51.6
2×10^{-5}	50.45°	96.6	0.5388	0.688	49.75°	98.1
4×10^{-5}	52.73°	177.0	0.5953	0.856	51.85°	185.8

Figures and Figure Captions

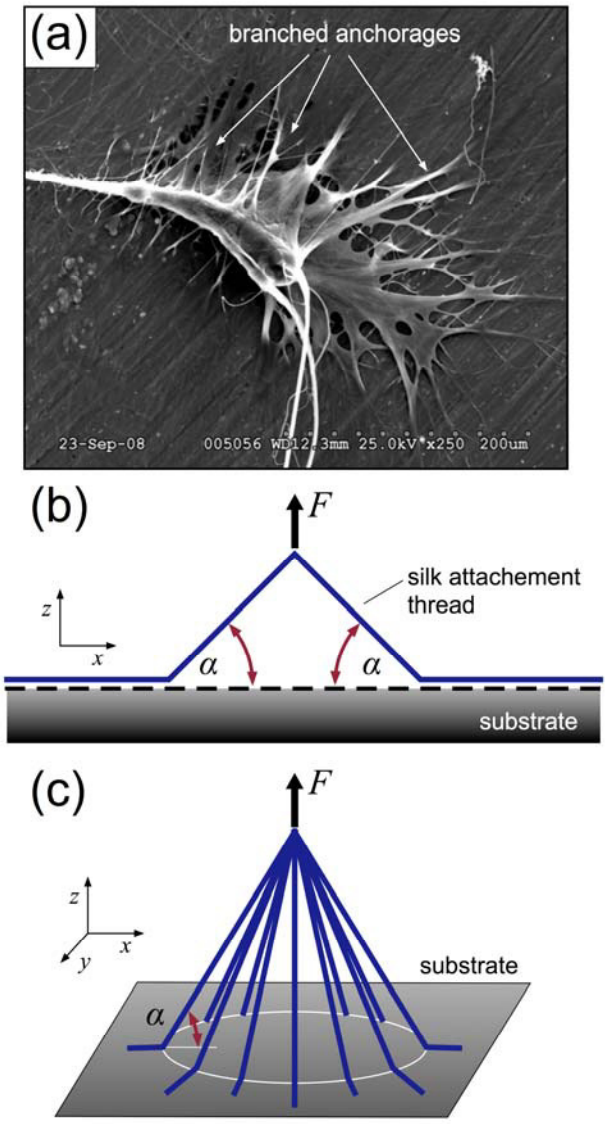

Figure 1: Structure of attachment discs anchoring a spider web to its environment. **(a),** SEM image of the attachment disc of a black-widow spider, *L. hesperus* (from ref.[9]). (**b),** A colarchic, two-branched adhesive anchorage (simple anchorage). The force *F* is applied perpendicularly to the substrate. **(c),** A great number of branches having identical lengths and contact angles arranged in a cone shape.

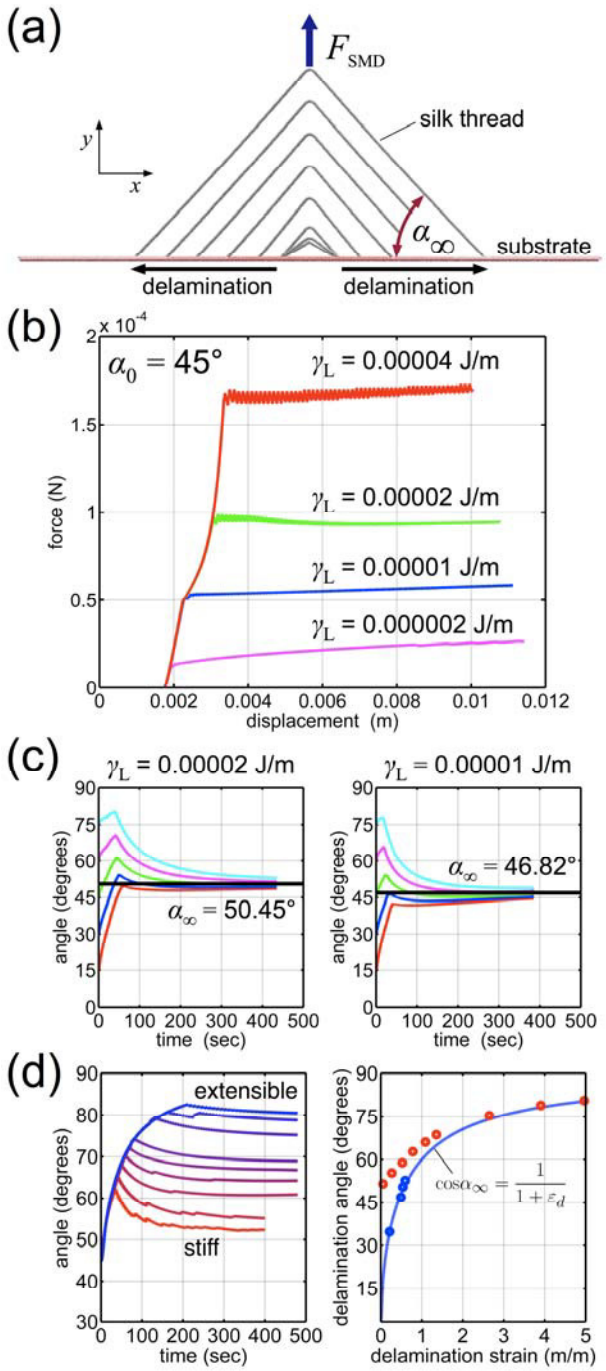

Figure 2: Summary of peeling simulations. **(a),** Silk model for two-branched peeling simulations in with prescribed adhesion energy, γ_L, and attachment angle, α_0. Snapshots depict evolution of attachment angle under load with $\alpha_0 = 30°$ and $\gamma_L = 2 \times 10^{-5}$ J/m (50 sec. increments). **(b),** Applied force versus attachment structure displacement, for $\alpha_0 = 45°$ and γ_L from 0.2×10^{-5} J/m to 4.0×10^{-5} J/m. **(c),** Measured angle versus times for peeling simulations with silk model for varying substrate

interaction values γ_L = 0.00002 J/m and γ_L = 0.00001 J/m; initial attachment angles, $\alpha_{0,}$ of 15°, 30°, 45°, 60°, and 75°; regardless of initial attachment angle, the detachment angle approaches an asymptotic value, α_∞, upon delamination (50.45° and 46.82° for 0.00002 J/m and 0.00001 J/m respectively). **(d)**, *Left*: Measured angle versus time for simulations with varying silk behaviors (hyperelastic model with ultimate strains from 0.1 (stiff) to 10.0 (extensible)), constant adhesion energy and initial attachment angle. *Right*: Delamination strain versus angle for all models. Points reflect measured asymptotic angles, α_∞; line indicates relation given by Eq. (5).

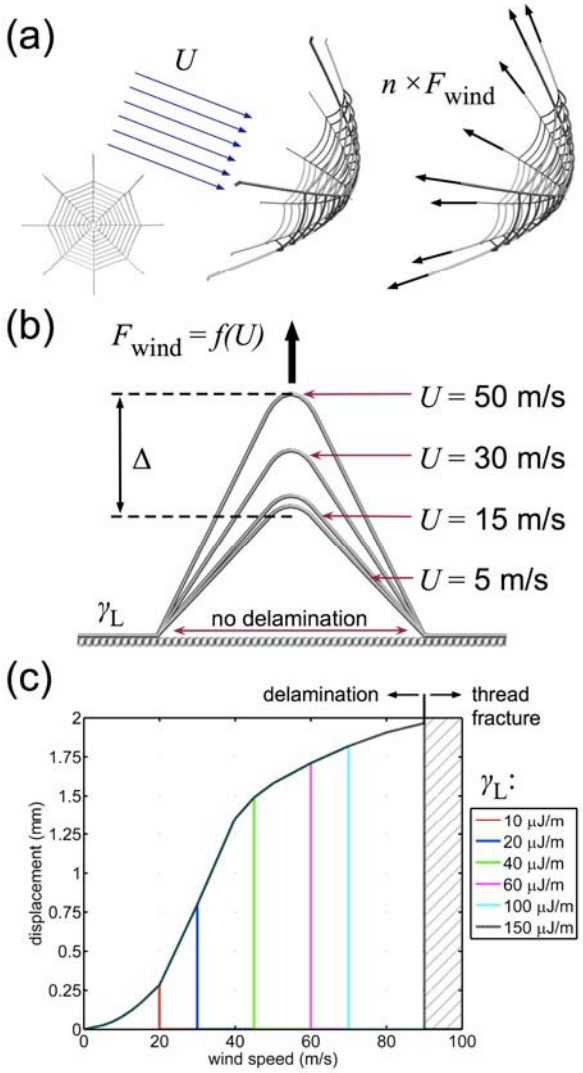

Figure 3: Summary of wind load simulations. **(a),** Derivation of equivalent anchorage forces derived by constant drag force resisted by an idealized model web. **(b),** Equivalent force (F_{wind}) is applied to the model as a function of wind speed, U, and total displacement, Δ, of the anchorage is measured upon equilibration. Snapshots depict an adhesion energy of γ_L = 60 μJ/m. **(c),** Plot of wind speed versus anchorage displacement with variation in adhesion energy (γ_L = 10 to 150 μJ/m). At small adhesion energies, delamination occurs at relatively small wind speed. While increasing adhesion energy and thread strength can prevent delamination further, ultimate failure (fracture) of the thread will occur when the adhesion energy is on the order of 150 μJ/m.

Table of contents entry

Synergetic material and structure optimization yields robust spider web anchorages
N.M. Pugno, S.W. Cranford, M.J. Buehler

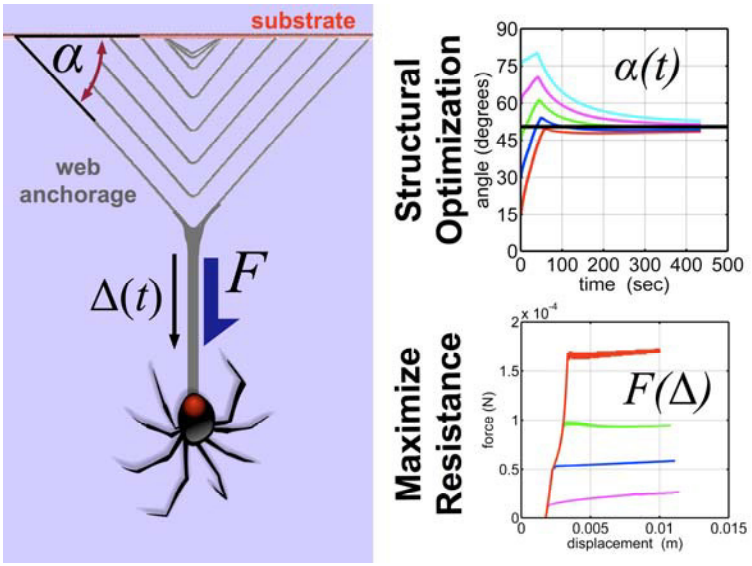

How does a spider attach a web to the environment, in spite of unknown conditions? The answer is the unique attachment disk, a clustered network of piriform silk fibers that mechanically anchors a web. Through integrated theoretical, computational, and experimental analysis, we elucidate a clever mechanism by which this structure provides a self-optimizing strong and robust attachment.

Supporting Information

Synergetic material and structure optimization yields robust spider web anchorages

Nicola M. Pugno, *Steven W. Cranford*, *Markus J. Buehler*

S1. Relating Optimal Strength, Strain, and Toughness

The optimal strength of the simple anchorage (the subscript "1" denotes properties which refer to this structure) with simultaneous material failure and delamination is:

$$F_1^{\mathrm{opt}} = 8\gamma \frac{\sqrt{\left(\varepsilon_{\mathrm{p}}^{\mathrm{opt}}\right)^2 + 2\varepsilon_{\mathrm{p}}^{\mathrm{opt}}}}{\left(\varepsilon_{\mathrm{p}}^{\mathrm{opt}}\right)^2 + 3\varepsilon_{\mathrm{p}}^{\mathrm{opt}}} \tag{S1}$$

The energetic capacity in the linear elastic domain of the simple structure which we are considering is:

$$\frac{T_1^{\mathrm{opt}}}{L} = 2\left(\frac{1}{2}\sigma_{\mathrm{p}}^{\mathrm{opt}}\varepsilon_{\mathrm{p}}^{\mathrm{opt}}A_{\mathrm{c}}\right) = 4\gamma\frac{1+\varepsilon_{\mathrm{p}}^{\mathrm{opt}}}{3+\varepsilon_{\mathrm{p}}^{\mathrm{opt}}} \tag{S2}$$

We denominate the energetic capacity T in reference to the material property "toughness" although here we discuss a structural property; L is the branch length. The energetic capacity increases asymptotically with yield strain ($\varepsilon_{\mathrm{p}}^{\mathrm{opt}}$) up to a value of 4γ.

Manipulation of Equations (S6) and (S7) to eliminate γ yields:

$$\frac{T_1^{\mathrm{opt}}}{L} = 4\gamma\frac{1+\varepsilon_{\mathrm{p}}^{\mathrm{opt}}}{3+\varepsilon_{\mathrm{p}}^{\mathrm{opt}}} = F_1^{\mathrm{opt}}\frac{\left(\varepsilon_{\mathrm{p}}^{\mathrm{opt}}\right)^2 + \varepsilon_{\mathrm{p}}^{\mathrm{opt}}}{2\sqrt{\left(\varepsilon_{\mathrm{p}}^{\mathrm{opt}}\right)^2 + 2\varepsilon_{\mathrm{p}}^{\mathrm{opt}}}} \tag{S3a}$$

From which it is apparent that:

$$T_1^{\mathrm{opt}} \to 4\gamma L \ \text{ as } \ \varepsilon_{\mathrm{p}}^{\mathrm{opt}} \to \infty \tag{S3b}$$

and

$$F_1^{\mathrm{opt}} \to 0 \ \text{ as } \varepsilon_{\mathrm{p}}^{\mathrm{opt}} \to \infty \tag{S3c}$$

S2. Contact Splitting

The total cross-sectional area is conserved between the cone and simple structures, that is $A_{\mathrm{c}} =$

Na_c, where a_c is the cross-sectional area of an individual branch, and N the total number of branches. The total strength, F_N, of the structure will be:

$$F_N = 2Y(Na_c)\sin\alpha\varepsilon_p \quad \text{(S4)}$$

Given that the critical delamination in our model (Equation (S1)) is equal to the value found by Kendall for single-branch peeling [31], we find our extension of the theory to higher values of N to be reasonable [16]. Consequently, the nondimensional parameter λ is increased by a factor of $\sqrt{N}$:

$$\lambda_N = \sqrt{N}\lambda_1 \quad \text{(S5a)}$$

and as a result the strength and the energetic capacity (if L is maintained constant) of the cone structure are increased by a factor of $\sqrt{N}$ with respect to the simple structure:

$$F_N = \sqrt{N}F_1 \quad \text{(S5b)}$$

$$T_N = \sqrt{N}T_1 \quad \text{(S5c)}$$

Finally we note that if conservation of material volume V is imposed between the cone and the simple anchorage (where $V = 2A_cL = 2Na_cL$). Substitution results in:

$$F_N = \frac{4\gamma}{a_c}\frac{\sqrt{\varepsilon_p^2+2\varepsilon_p}}{\varepsilon_p^2+3\varepsilon_p}\frac{V}{L} \quad \text{(S6a)}$$

and

$$T_N = \frac{2\gamma}{a_c}\frac{1+\varepsilon_p}{3+\varepsilon_p}V \quad \text{(S6b)}$$

where a_c is the cross-sectional area of a individual branch, and N the total number of branches ($A_c = Na_c$,), and the volume, $V = A_cL$.

S3. SEM Observations and Predictions

In the SEM photograph of the attachment disk of a black widow spider published by Blasingame *et al*. [9] (**Figure 1a**), we make an approximation of the total number of fibrils in contact with the substrate. We count that 10 fibrils are found in a space of about 200 μm^2 and the total area of the anchorage, approximately equal to the area of the photograph, is 200,000 μm^2. We therefore arrive at the estimate that there are on the order of 10,000 fibrils in contact with the substrate, fibrils which the authors report to have a circular cross-section of diameter around 0.4 μm ($r \cong 0.2$ μm). Consequently the sum of the cross-sections will be (we use the superscript "ad*"* for properties which refer to the attachment disk):

$$A_c \cong 10{,}000 \times \pi r^2 \cong 1 \times 10^{-9}\text{m}^2$$

For a first-order estimate of mechanical properties, we assume that the lower bound strength of the attachment disk for a particular spider should be on the order of its weight, *e.g.* $F^{\mathrm{ad}} \approx 0.01$ N (1g mass). We further estimate that the energy of adhesion will be approximately 10 N/m. (e.g., contact length of 1 mm to bear the spider) and subsequently, for a characteristic contact width on the order of a micrometer, $\gamma \approx 10^{-5}$ J/m. We estimate the silk stiffness assuming linear elastic behavior (albeit, unlikely for silk), where $Y^{\mathrm{ad}} \cong 3$ MPa, a measured initial stiffness of viscid (capture) silks [10]. Compared to the initial stiffness of dragline silk ($Y^{\mathrm{dragline}} \approx 10$ GPa [10]) this is a low elastic modulus. We find that the material extensibility must be: $\varepsilon_{\mathrm{p}}^{\mathrm{ad}} \cong 3.4$. This subsequently leads to a very high optimal branch-substrate angle (as per Equation (2)): $\alpha^{\mathrm{ad}} \cong 77°$. We note the inherent nonlinear tensile behavior of silk (typically hyperlastic stiffening), limits a more exact prediction. Considering the extensibility is much higher than that of the dragline ($\varepsilon_{\mathrm{p}}^{\mathrm{dragline}} \approx 0.5$ [10]), it can be presumed that piriform silk will also reflect hyperelastic stiffening. Of course these represent only preliminary and rough estimation of the still unknown piriform silk.

S4. Calculation of λ

Due to the nonlinear behavior of the silk, we let $YA = F_{\mathrm{silk}}/\varepsilon_{\mathrm{silk}}$, where F_{silk} is the force in the silk thread at delamination (the measured value of F_{d}), which is constant independent of initial attachment angle, calculated by the applied force, F_{SMD}, where:

$$F_{\mathrm{silk}} = 0.5\, F_{\mathrm{SMD}}/\sin\alpha_{\infty} \tag{S7}$$

and $\varepsilon_{\mathrm{silk}}$ is the associated strain in the silk at the limiting force (from the constitutive behavior defined). Consequently, calculation of λ is slightly modified to an equivalent form:

$$\lambda = 4\gamma\varepsilon_{\mathrm{silk}}/F_{\mathrm{silk}} \tag{S8}$$

from which we calculate λ for each level of adhesion strength, γ, based on the simulation results (**Table 1**).

S5. Silk model(s)

A. Atomistically derived generalized silk model

A combination linear and exponential function is used to reflect the characteristic nonlinear stress-strain behavior of the silk, accounting for the molecular make-up [4, 19]. The exponential function depicted expresses the simultaneous unfolding behavior of the amorphous regime and the transfer of load to the stiffer β-sheet nanocrystals. The function is expressed as:

$$\sigma(\varepsilon) = \begin{cases} E_1\varepsilon & , 0 \le \varepsilon < \varepsilon_y \\ \exp\left[k_1(\varepsilon - \varepsilon_y)\right] + k_2(\varepsilon - \varepsilon_y) + C_1 & , \varepsilon_y \le \varepsilon < \varepsilon_s \\ E_2(\varepsilon - \varepsilon_s) + C_2 & , \varepsilon_s \le \varepsilon < \varepsilon_b \\ 0 & , \quad \varepsilon \ge \varepsilon_b \end{cases} \tag{S9}$$

defined by four parameters (E_1, E_2, k_1, and k_2) reflecting stiffness, and three corresponding to critical strains (ε_y, ε_s, ε_b) given in **Table S1**. The constants, C_1 and C_2, ensure continuity between the linear and exponential regimes. For tensile stretching, the stress-strain behavior is converted to a force-displacement spring function by the geometry of the web model, to allow a coarse-grain molecular dynamics implementation. We find that the resulting stress-strain curve displays the characteristic shape observed in silk [10, 32], that is, an early yield point with associated softening, followed by a severe stiffening effect, until failure, depicted in **Figure S1.**

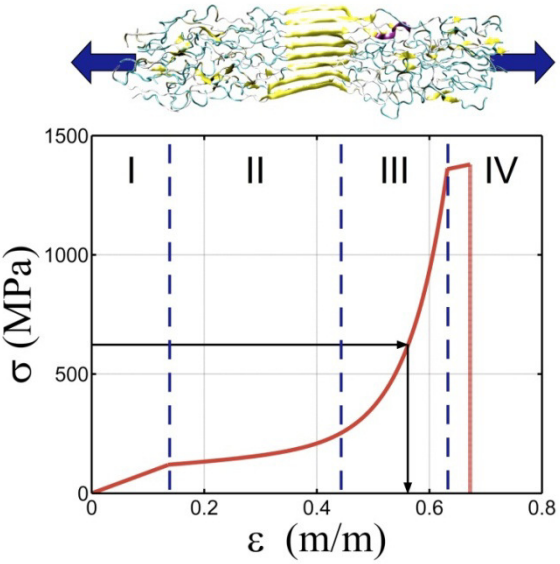

Figure S1: Derived constitutive behavior parameterized from full atomistic simulations of dragline spider silk and validated against experimentally measured behaviors [19]. Schematic depicts the molecular nanostructure under deformation, which accounts for the combined behavior of beta-sheet nanocrystals [19c] and semi-amorphous protein domains [19a]. Arrows indicate the simple procedure for determining the strain at detachment, ε_{silk}, if the force F_{silk} is known (where $\sigma = F/A$).

To maintain *de facto* independence from empirical data, only the molecular behavior is considered for model parameterization. Being said, the maximum stress level, on the order of 1-2 GPa, is in quantitative agreement with results from experimental studies [32].

As previously stated, in spiders, dragline, capture and piriform silks are produced independently and differ in their detailed molecular structure. Dragline threads are produced by the major ampullate glands [33] whereas these gluey "attachment silks" originate from the piriform glands [2a, 34]. Nevertheless silks express a universal characteristic mechanical behavior, and the ultimate stresses attained by silks are comparable in magnitude. As earlier full atomistic investigations were undertaken with dragline silk molecular structures [19a, 19c, 35], it is a simplifying assumption of the attachment model that this behavior is also sufficiently reflective of piriform silk. Our model allows the dynamic simulation of the attachment structure, as well as associated deformation and failure mechanisms.

Table S1: Silk model stress-strain behavior parameters

Parameter	Value
Initial stiffness, E_1	875.9 MPa
Exponential parameter, k_1	14.2
Tangent stiffness parameter, k_2	180 MPa
Final stiffness, E_2	491.2 MPa
Yield strain, ε_y	0.1356
Softening strain, ε_s	0.6322
Ultimate (breaking) strain, ε_b	0.6725
Thread diameter	0.4 μm

B. General hyperelastic silk model w/ variable extensibility

To test the validity of our theoretical predictions (namely, the relationship between optimal detachment angle, α_{max}, and delamination strain, ε_d, as given by Eq. (3)), we introduce a generalized hyperelastic constitutive law (similar to the behaviour of capture, or viscid, silks [10, 27a]), which can systematically be varied from a relatively stiff, brittle response ($\varepsilon_{ult} = 0.1$), to a highly compliant, extensible response ($\varepsilon_{ult} = 10.0$). For all models, the strength (ultimate stress) is equivalent (σ_{ult} = 1379 MPa). The material law is expressed as:

$$\sigma(\varepsilon) = \sigma_{\text{ult}} \left(\frac{\varepsilon}{\varepsilon_{\text{ult}}}\right)^{\alpha} \tag{S10}$$

defined by three parameters: ultimate stress (σ_{ult} = *constant* = 1379 MPa), ultimate strain (ε_{ult} = 0.10, 0.25, 0.50, 1.00, 1.50, 2.00, 2.50, 5.00, 7.50, 10.00), and a nondimensional hyperelastic parameter, α (here, α = 3.0). The material laws are depicted in **Figure S2**.

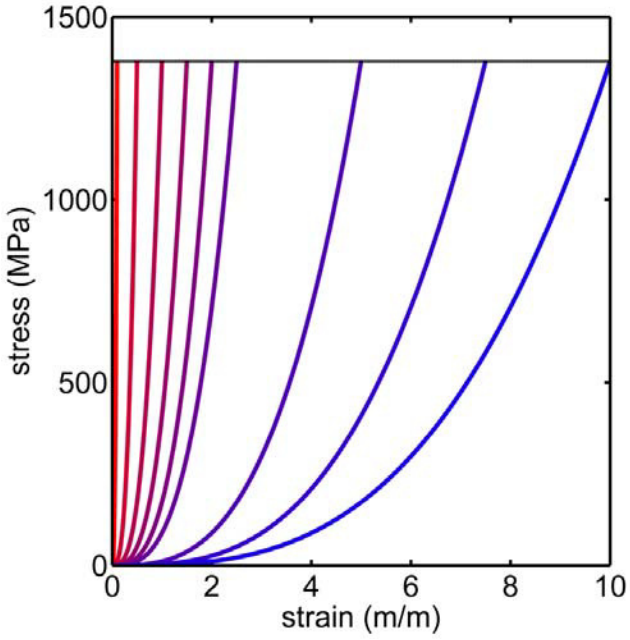

Figure S2: Generalized hyperelastic silk model with variable stiffness/extension. Ultimate strains range from 0.1 to 10.0, with a constant ultimate stress (1,379 MPa) as indicated.

S6. Substrate Adhesion

We introduce a single silk thread with a total length of 45 mm, of which 40 mm (two 20 mm branches) is attached to a rigid substrate with a Lennard-Jones interaction of the type:

$$E = 4\varepsilon\left[\left(\frac{\sigma}{r}\right)^{12} - \left(\frac{\sigma}{r}\right)^{6}\right] \text{ for } r < r_{cut} \qquad \text{(S11)}$$

where E is the energy of the interaction, ε is the adhesion parameter, σ an interaction-range parameter, r is the distance between the two particles, and r_{cut} is the cutoff-distance beyond which the interaction no longer has effect. We use σ = 0.089 mm, leading to an energy minimum at a spacing 0.1 mm and r_{cut} = 0.50 mm. The adhesion parameter, ε, is proportional to the energy of adhesion per unit length of silk, γ_L, and is a variable in these simulations, taking on the values γ_L ranging from 0.2×10^{-5} to 2×10^{-5} J/m.

S7. Wind Loading

From previous modeling of a complete idealized web structure, the force transferred to each two branch anchorage can be estimated. To model the force due to wind, we utilize the effect of drag on the silk threads, similar to the wind drag on cable bridges [36]. The static drag wind load on a structural cable is written as:

$$F_{\mathrm{d}} = \frac{1}{2}\rho_{\mathrm{air}} U^2 C_D A_{web} \qquad \text{(S12)}$$

where ρ_{air} is the air density (1.15 kg/m^2), U a mean wind speed, C_D the drag coefficient in the along-wind direction (conservatively taken as 1.2, typical value for structural wires and cables [36]), and A_{web} the reference area of the silk threads that compose the web, where:

$$A_{web} = \sum_i A_i \text{ and } A_i = L_i \times d_i \quad \text{(S13)}$$

Here, the subscript *"i"* refers to the two different silk types that compose a common web: dragline silk that constitutes the radial (load bearing) threads, and viscid silk that constitutes the spiral (capture) threads of a typical orb web [10, 37]. For the diameters of the silk threads, we use 3.93 μm and 2.40 μm for radial and spiral threads respectively [33b, 38]. We assume a thread diameter of 0.4 μm for anchor threads, and each radial thread is equally divided into 96 adhered branches. The calculated load is applied *via* constant force SMD for 100 seconds.

Supporting References

[31] Kendall, K., *J Phys D Appl Phys* **1975,** *8* (13), 1449-1452.
[32] Du, N.; Liu, X. Y.; Narayanan, J.; Li, L. A.; Lim, M. L. M.; Li, D. Q., *Biophysical Journal* **2006,** *91* (12), 4528-4535. DOI DOI 10.1529/biophysj.106.089144.
[33] a) Kohler, T.; Vollrath, F., *Journal of Experimental Zoology* **1995,** *271* (1), 1-17; b) Lin, L. H.; Sobek, W., *The Structural Engineer* **1998,** *76* (4), 59-64; c) Vollrath, F., *Reviews in Molecular Biotechnology* **2000,** *74*, 67-83.
[34] a) Romer, L.; Scheibel, T., *Prion* **2008,** *2* (4), 154-161; b) Heim, M.; Keerl, D.; Scheibel, T., *Angewandte Chemie-International Edition* **2009,** *48* (20), 3584-3596. DOI DOI 10.1002/anie.200803341; c) Heim, M.; Romer, L.; Scheibel, T., *Chemical Society Reviews* **2010,** *39* (1), 156-164. DOI Doi 10.1039/B813273a.
[35] Keten, S.; Buehler, M. J., *Appl Phys Lett* **2010,** *96* (15). DOI Artn 153701 Doi 10.1063/1.3385388.
[36] Poulin, S.; Larsen, A., *Journal of Wind Engineering and Industrial Aerodynamics* **2007,** *95* (9-11), 1350-1363. DOI DOI 10.1016/j.jweia.2007.02.011.
[37] Vollrath, F.; Mohren, W., *Naturwissenschaften* **1985,** *72* (12), 666-667.
[38] Alam, M. S.; Wahab, M. A.; Jenkins, C. H., *Mechanics of Materials* **2007,** *39* (2), 145-160.

This is the pre-peer reviewed version of the following article:

Pugno N. M., Cranford S.W., Buehler M. J., Synergetic Material and Structure Optimization Yields Robust Spider Web Anchorages, *Small*, 9(16):2747-2756, 2013

which has been published in final form at

http://onlinelibrary.wiley.com/doi/10.1002/smll.201201343/full.